DC Link Voltage and Power Flow Control of a Doubly Fed Induction Generator in Wind Power System

Milkias Berhanu

Department of Electrical Power and Control Engineering
Adama Science and Technology University
Adama, Ethiopia
mil_ber2000@astu.edu.et

Roberto Leidhold
Institute of Electric Power Systems
Otto-Von-Guericke University
Magdeburg, Germany
roberto.leidh0ld@ovgu.de

Abstract—Doubly Fed Induction Generator (DFIG) is the most commonly used type of induction generators nowadays in wind power industry where it is connected with grid directly through its stator and via dual-back-to-back converters through the rotor. This paper focuses on its modeling and control of DC link voltage and the power flow between the generator and the grid. The effects of load current transients and reactive power changes are analyzed. To meet the target, the machine side converter (MSC) is modeled to regulate the stator active and reactive power whereas the grid side converter (GSC) ensures the regulation of the DC link voltage. The pulse-width modulation (PWM) strategy is used to control the two converters in dq frames. PI controllers are designed and applied in two reference frames: one oriented with the stator flux and the other with grid voltage, for the MSC and GSC respectively. MATLAB-Simulink software is used for modelling, simulation, and control.

Key words: Active and Reactive power, DC bus, DFIG, MATLAB-Simulink

I. INTRODUCTION

This paper is prepared aiming to achieve a well modeled DFIG and its control strategy to study optimal power flow in a wind farm that is important to analyze it in any abnormal conditions. Many countries, especially in the developing parts of the world, have considerable wind resources that are still untapped due to their lack of expertise, concerning both methods of site selection and technical aspects of wind power [1]. Ethiopia has good wind resources with average velocities ranging from 7 to 9 m/s with wind energy potential estimated to be 10 GW while the current installed capacity is 324 MW [2]. The DFIG installed in Adama-II wind farm of Ethiopia is used under the study. Once its model is well developed, the machine's operating states at various conditions can be analyzed.

II. DOUBLY-FED INDUCTION GENERATOR (DFIG) AND ITS BACKGROUND

DFIG which can operate as a generating/motoring mode coupled with the grid at constant amplitude and frequency through its stator and via converters at its rotor can be drawn as shown in Fig.1 [3] where GB stands for gear box and WT for wind turbine.
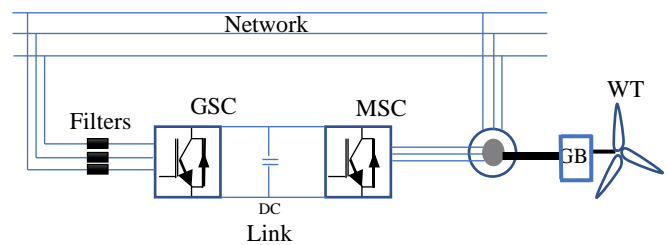

Fig.1. Doubly-fed induction generator in wind power system.

Depending on the sign of the slip, the DFIG can work in super-synchronous/sub-synchronous modes of operation. The rotor delivers power to the grid during super-synchronous mode of operation and receives it during sub-synchronous mode of operation. As a result, the total power sent to the grid, that is the algebraic sum of the stator and rotor power is varying. DFIG which is also called a wound-rotor induction generator, is most commonly used in wind farms due to its reduced converter size near 30% of rated value and other advantages like unity power factor control. The upcoming section discuss its modelling & control techniques.

III. MODELING DOUBLY-FED INDUCTION GENERATOR

In order to carry out various analyses on the DFIG under steady state and dynamic conditions for optimal operation and control, its modelling is very important.

A. Wind Turbine (WT) Model

WTs are used to produce electricity by using the power of the wind to drive an electrical generator. As Wind passes over the blades, generating lift and exerting a turning force. The rotating blades turn a shaft inside the nacelle, which goes into a gearbox that increases the rotational speed appropriate for the generator [3]. The power of an air mass of wind in the form of kinetic energy crossing at a speed (V_v) in m/s through a swift area (A) in m^2 is:

$$P_v = \frac{1}{2}\rho A V_v^3 \tag{1}$$

Where, ρ is air density (kg/m^3) =1.225 kg/m^3

Only a portion of power in air can be recovered by a wind turbine. Considering the efficiency, the wind power captured by the blade and converted into mechanical power can be calculated:

$$P_t = \frac{1}{2}\rho A V_v^3 C_p = \frac{1}{2}\rho \pi R^2 V_v^3 C_p \qquad (2)$$

$A = \pi R^2$, where R is the radius of WT or length of the blades (m), C_p is power coefficient. C_p is often given as a function of the tip speed ratio, λ, defined by [3]:

$$\lambda = \frac{\omega_t R}{V_v} \qquad (3)$$

ω_t = is the angular speed of the rotor (rad/s)
The rotor torque is obtained from the power received and the speed of rotation is given by:

$$T_t = P_t/\omega_t = \frac{1}{2}\rho \pi R^2 \frac{V_v^2}{\omega_t}C_p = \frac{1}{2}\rho \pi R^3 \frac{V_v^2}{\lambda}C_p \qquad (4)$$

The wind speed can be considered as the averaged incident wind on the swept area by the blades with the aim of evaluating the average torque in the low speed axle.

B. Modelling for Maximum Power Tracking

In the time when the wind speed is in the range of cut-in and rated value, the maximum aerodynamic power available in the wind can be captured. The maximum power in a mass of wind can be extracted by varying the turbine speed with the varying wind speed so that at all times it is on the track of the maximum power curve [4]. For efficient wind power captured by the variable wind turbine, λ =λ_{opt}. Therefore, tip speed ratio can be re-written as,

$$\lambda_{opt} = \frac{\omega_t R}{V_v} \rightarrow V_v = \frac{\omega_t R}{\lambda_{opt}} \; ; \& \; C_{p-max} = C_p(\lambda_{opt}) \qquad (5)$$

The aerodynamic torque extracted by the WT is then given by:

$$T_t = \frac{1}{2}\rho \pi R^3 \frac{R^2 \omega_t^2}{\lambda_{opt}^2}\frac{C_{p,max}(\lambda_{opt},\theta=0)}{\lambda_{opt}} = \frac{1}{2}\rho \pi \frac{R^5}{\lambda_{opt}^3}C_{p,max}(\lambda_{opt}, \theta = 0)\omega_t^2 \quad (6)$$

By substitution, optimum power can be obtained as,

$$P_{opt} = \frac{1}{2}\rho \pi R^2 V_v^3 C_p = \frac{1}{2}\frac{\rho \pi R^2 C_{p,max}(\lambda_{opt}, \theta = 0)R^3}{\lambda_{opt}^3}\omega_t^3 = \frac{1}{2}\rho \pi R^5 \frac{C_{p,max}(\lambda_{opt}, \theta = 0)}{\lambda_{opt}^3}\omega_t^3 (7)$$

In this study, λ_{opt} = 9 and $C_{p,max}$ = 0.4865 are used [6].
The above equations are used in embedded MATLAB function for simulation and analyses.

C. Dynamic Models

i. αβ Model

In developing the dynamic αβ model of the DFIM, space vector theory is applied to the basic electric equations of the machine. Fig. 2 shows the three different rotating reference frames typically utilized to develop space vector-based models of the DFIM. The stator reference frame (α-β) is a stationary reference frame, the rotor reference frame (*DQ*) rotates at ω_m and the synchronous reference frame (dq) rotates at ω_s. Subscripts "s", "r" and "a" are used to denote that one space vector is reference to the stator, rotor and synchronous reference frames, respectively. By using Clark and park

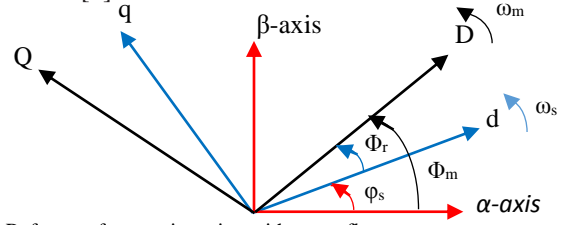transformations, a space vector can be represented in any of these frames [3]

Fig. 2. Reference frame orientation with stator flux.

Hence, the three windings of the stator and rotor can be represented separately by using a space vector theory on two stationary αβ coils for the stator and two rotating coils *DQ* for the rotor, giving the following voltage equations:

$$\vec{V}_s^s = [\vec{Is}^s][R_s] + \frac{d\left|\vec{\psi}_s^s\right|}{dt} \; ; \vec{V}_r^r = [\vec{I}_r^r][R_r] + \frac{d\left|\vec{\psi}_r^r\right|}{dt} \qquad (8)$$

If both voltage equations are represented in stationary reference frame αβ, then the rotor equation must be multiplied by $e^{j\theta m}$, which yields the following set of equations [5]:

$$\vec{V}_s^s = [\vec{Is}^s][R_s] + \frac{d\left|\vec{\psi}_s^s\right|}{dt} \Rightarrow \begin{cases} v_{\alpha s} = r_s i_{\alpha s} + \dfrac{d\psi_{\alpha s}}{dt} \\ v_{\beta s} = r_s i_{\beta s} + \dfrac{d\psi_{\beta s}}{dt} \end{cases} \qquad (9)$$

Writing the rotor voltage in stator reference frame:

$$\vec{V}_r^s = [\vec{i}_r^s][R_r] + \begin{bmatrix} 0 & 1 \\ -1 & 0 \end{bmatrix}\omega_m \cdot \vec{\psi}_r^s + \frac{d\vec{\psi}_r^s}{dt} \Rightarrow \begin{cases} v_{\alpha r} = R_r i_{\alpha r} + \dfrac{d\psi_{\alpha r}}{dt} + \omega_m \psi_{\beta r} \\ v_{\beta r} = R_r i_{\beta r} + \dfrac{d\psi_{\beta r}}{dt} - \omega_m \psi_{\alpha r} \end{cases} \qquad (10)$$

The stator and rotor flux expressions in space vector form in a stationary reference frame:

$$\begin{bmatrix} \psi_s^s \\ \psi_r^s \end{bmatrix} = \begin{bmatrix} L_s & L_m \\ L_m & L_r \end{bmatrix} \cdot \begin{bmatrix} i_s^s \\ i_r^s \end{bmatrix} \rightarrow \begin{cases} \psi_{\alpha s} = L_s i_{\alpha s} + L_m i_{\alpha r} \\ \psi_{\beta s} = L_s i_{\beta s} + L_m i_{\beta r} \\ \psi_{\alpha r} = L_m i_{\alpha s} + L_r i_{\alpha r} \\ \psi_{\beta r} = L_m i_{\beta s} + L_r i_{\beta r} \end{cases} \qquad (11)$$

$$\begin{bmatrix} i_s^s \\ i_r^s \end{bmatrix} = \frac{1}{L_m^2 - L_s L_r}\begin{bmatrix} -L_r & L_m \\ L_m & -L_s \end{bmatrix}\begin{bmatrix} \psi_s^s \\ \psi_r^s \end{bmatrix} = K.\begin{bmatrix} -L_r & L_m \\ L_m & -L_s \end{bmatrix}\begin{bmatrix} \psi_s^s \\ \psi_r^s \end{bmatrix} \qquad (12)$$

Where, $K = \dfrac{1}{L_m^2 - L_s.L_r}$; $L_s = L_{ls} + L_m$; and $L_r = L_{lr} + L_m$

$v_{\alpha s}$, $v_{\beta s}$, $i_{\alpha s}$, $i_{\beta s}$, $i_{\alpha r}$, $i_{\beta r}$ and $\psi_{\alpha s}$, $\psi_{\beta s}$, $\psi_{\alpha r}$, $\psi_{\beta r}$, are voltages (V), currents (A) and flux linkages (Wb) of the stator and rotor in αβ-axis, R_s and R_r are resistances of the stator and rotor windings (Ω), L_s, L_r, L_m are the stator, rotor and mutual inductances (H). L_{ls}, L_{lr} are the stator and rotor leakage inductances (H), ω is the speed of the reference frame (rad/s), ω_m is the mechanical angular velocity of the generator rotor (rad/s). The values of the above parameters are obtained from the factory test reports, nameplate and numerical analysis [6], [7].

On the other hand, the stator and rotor active and reactive power can be given by [5]:

$$P_s = \frac{3}{2}(v_{\alpha s}i_{\alpha s} + v_{\beta s}i_{\beta s}) \quad P_r = \frac{3}{2}(v_{\alpha r}i_{\alpha r} + v_{\beta r}i_{\beta r}) \quad (13)$$

$$Q_s = \frac{3}{2}(v_{\beta s}i_{\alpha s} - v_{\alpha s}i_{\beta s}) \quad Q_r = \frac{3}{2}(v_{\beta r}i_{\alpha r} - v_{\alpha r}i_{\beta r}) \quad (14)$$

Whereas, the electromagnetic torque developed by the DFIG can be calculated by:

$$T_{em} = \frac{3}{2}pI_m\{\vec{\psi}_r \vec{i}_r\} = \frac{3}{2}p(\psi_{\beta r}i_{\alpha r} - \psi_{\alpha r}i_{\beta r}) \quad (15)$$

Where, p is number of pole pairs:
By taking the mechanical load torque (T_m) applied to the shaft as developed by wind speed variations to describe the dynamic motion of the rotor:

$$T_{em} - T_m = J\frac{d\omega_m}{dt} \quad (16)$$

Where, J is the sum of inertia of the WT and generator (J_g). The individual J_t and J_g are obtained. The rated speed of DFIG is 1800 rpm and ω_t rated is 19 rpm and hence G is 94.7[6], [7].

ii. dq Axis Model

The space vector model of the DFIG can also be represented in a synchronously rotating frame by multiplying the voltage expressions by $e^{-j\theta s}$ and $e^{-j\theta r}$ for stator and rotor respectively. As a result, the dq voltage equations can be [5]:

$$\vec{V}_s^r = \vec{I}_s^r R_s + \frac{d\vec{\psi}_s^r}{dt} + j\vec{\omega}_s^r \rightarrow \begin{cases} v_{ds} = R_s i_{ds} + \dfrac{d\psi_{ds}}{dt} - \omega_s\psi_{qs} \\[2mm] v_{qs} = R_s i_{qs} + \dfrac{d\psi_{qs}}{dt} + \omega_s\psi_{ds} \end{cases} \quad (17)$$

$$\vec{V}_r^r = \vec{I}_r^r R_r + \frac{d\vec{\psi}_r^r}{dt} + j\vec{\omega}_r^r \rightarrow \begin{cases} v_{dr} = R_r i_{dr} + \dfrac{d\psi_{dr}}{dt} - \omega_r\psi_{qr} \\[2mm] v_{qr} = R_r i_{qr} + \dfrac{d\psi_{qr}}{dt} + \omega_r\psi_{dr} \end{cases} \quad (18)$$

Where $\omega_r = \omega_s - \omega_m$. Similarly, the fluxes yield:

$$\begin{bmatrix} \psi_s^r \\ \psi_r^r \end{bmatrix} = \begin{bmatrix} L_s & L_m \\ L_m & L_r \end{bmatrix} \cdot \begin{bmatrix} i_s^r \\ i_r^r \end{bmatrix} \rightarrow \begin{cases} \psi_{ds} = L_s i_{ds} + L_m i_{dr} \\ \psi_{qs} = L_s i_{qs} + L_m i_{qr} \\ \psi_{dr} = L_m i_{ds} + L_r i_{qr} \\ \psi_{qr} = L_m i_{qs} + L_r i_{qr} \end{cases} \quad (19)$$

The torque and power expressions in the dq reference frame [3], [5]:

$$P_s = 1.5(v_{ds}i_{ds} + v_{qs}i_{qs}) ; P_r = 1.5(v_{dr}i_{dr} + v_{qr}i_{qr}) \quad (20);$$

$$P_g = P_s + P_r = 1.5(v_{ds}i_{ds} + v_{qs}i_{qs} + v_{dr}i_{dr} + v_{qr}i_{qr}) \quad (21)$$

$$Q_s = 1.5(v_{qs}i_{ds} - v_{ds}i_{qs}) \quad Q_r = 1.5(v_{qr}i_{dr} - v_{dr}i_{qr}) \quad (22);$$

$$Q_g = Q_s + Q_r = 1.5\left[v_{qs}i_{ds} + v_{qr}i_{dr} - (v_{ds}i_{qs} + v_{dr}i_{qr})\right] \quad (23)$$

$$T_{em} = 1.5p(\psi_{dr}i_{qs} - \psi_{qr}i_{ds}) = 1.5pLm(i_{dr}i_{qs} - i_{qr}i_{ds}) \quad (24)$$

The power losses accompanied with the stator, rotor windings, and saturations are neglected.

IV. VECTOR CONTROL OF DFIG WITH PWM CONVERTERS

Dynamic control of the DFIG aiming to extract maximum power from the wind is provided through dual back-to-back power converters, which allows variable-speed operation of the wind turbine by decoupling the power system electrical frequency and the rotor mechanical speed [8]. In a vector control of DFIM, the components of the d and the q axis of the rotor current are regulated. A reference frame orientated with the stator flux as shown in Fig. 3 is used for the MSC. The active power and reactive power flows of the stator can be controlled independently by means of the quadrature and the direct current respectively [3], [5].
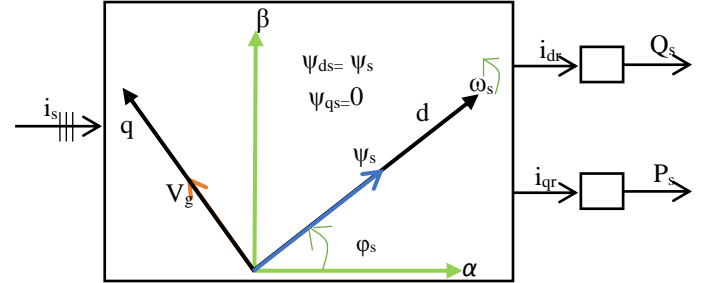

Fig. 3. Reference frame aligned with the stator flux

Under the rotor current control mode, stator flux is:

$$\psi_s = L_s i_{ds} + L_m i_{dr} ; \qquad 0 = L_s i_{qs} + L_m i_{qr} \quad (25)$$

$$i_{ds} = \frac{\psi_s - L_m}{L_s}i_{dr} \text{ and } i_{qs} = -\frac{L_m}{L_s}i_{qr} \quad (26)$$

In steady state, the stator flux is proportional to the grid voltage, V_g. Neglecting the small drop in the stator resistance; yields [3]:

$$V_{ds}=0; \quad V_{qs}= V_g \approx \omega_s\psi_s \quad (27)$$

Thus, with this orientation, the grid voltage aligns with the quadrature axis. By combining equations 25-27, the stator active and reactive power flow can then be re-written as:

$$P_s = -1.5\hat{V}_g \frac{L_m}{L_s}i_{qr} \quad (28)$$

$$Q_s = 1.5\hat{V}_g\left[\frac{\psi_s}{L_s} - \frac{L_m}{L_s}i_{dr}\right] = 1.5\hat{V}_g\left[\frac{\hat{V}_g}{\omega_s L_s} - \frac{L_m}{L_s}i_{dr}\right] \quad (29)$$

The GSC is modelled with the concept of grid voltage orientation in which the d-axis of the synchronous frame is aligned with grid voltage vector as shown in Fig. 4. Therefore, the d-axis grid voltage is equal to its magnitude ($v_{dg}=v_g$), and the resultant q-axis voltage v_{qg} is then equal to zero, from which the active and reactive power of the system can be computed [3]. The total active and reactive powers exchanged with the grid are calculated:

$$P_g = \frac{3}{2}(v_{dg}i_{dg} + v_{qg}i_{qg}) = \frac{3}{2}v_{dg}i_{dg} \quad (30)$$

$$Q_g = \frac{3}{2}(v_{qg}i_{dg} - v_{dg}i_{qg}) = -\frac{3}{2}v_{dg}i_{qg} \quad (31)$$

Thus, the i_{dg} current is responsible for the P_g value, while the i_{qg} current is responsible for the Q_g value. This fact is exploited in the control of the grid side system.
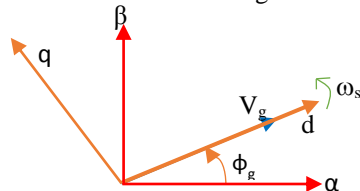

Fig. 4. Alignment of grid voltage space vector along d axis

V. DC LINK MODELLING

The DC part of the back-to-back converter is typically called the DC link and the energy stored in a capacitor(s) maintains a constant voltage in its terminals. It is the linkage between the grid side and rotor side converters. Fig. 5 shows a simplified model of DC link [3], [9]-[10].

$$V_{bus} = \frac{1}{C_{bus}} \int i_c dt$$

$$i_c = i_{dc,r} - i_{dc,g} - i_{res}$$
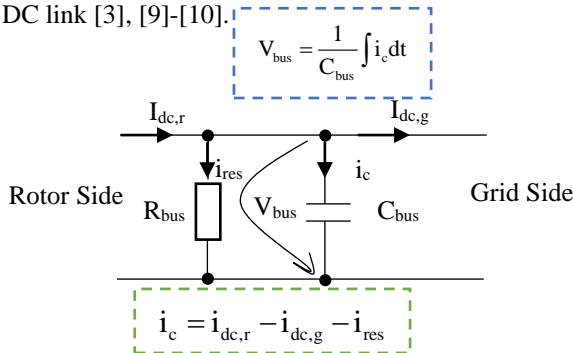
Fig. 5 Simplified model of a DC link.

Where i_{res}, $i_{dc,r}$ & $i_{dc,g}$ are currents through the resistance, DC current flowing from the rotor to the DC link, and DC current flowing from the DC link to the grid (A) respectively. The DC voltage control is done by the control of power exchanged through the converter with the grid. In this case, the decrease or increase of the DC voltage level is obtained by injecting more or less power to the grid with respect to that produced by the WTG, thus changing the value of the reference for the AC current control loop or the phase displacement of the AC voltage across the capacitor of the filter. The simplified diagram of DC link with both side converters is shown in Fig. 6.
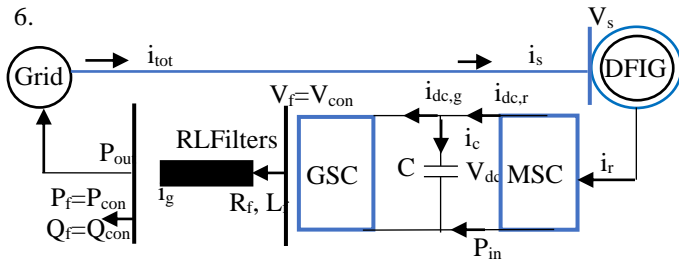

Fig. 6. DC link with both side converters

VI. RESULTS AND DISCUSSIONS

This section discusses the results obtained from the modelling and simulation computed in embedded MATLAB Simulink function as a simplified and masked model shown in Fig. 7. For this purpose, the DFIG with 690 V LL rms stator voltages, 50 Hz frequency together with other necessary real parameters obtained through numerical analysis and factory test reports are used. The assumed and averaged variable wind speed [6, 6, 10, 10, 6, and 6] is applied using the repeating sequence of the MATLAB over 30 seconds of the simulation period as the resulting generator speed is shown in Fig. 8.
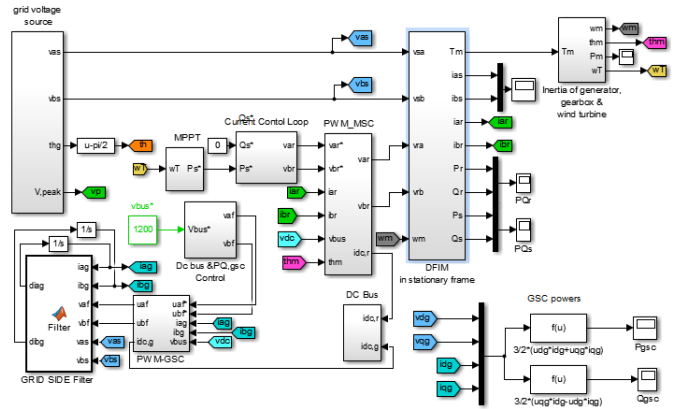

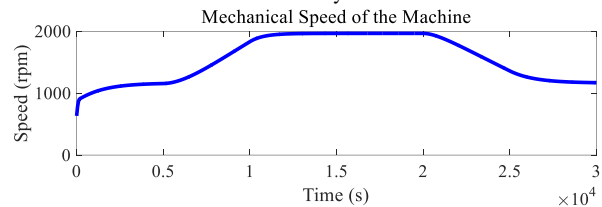Fig. 7 The simplified and masked embedded MATLAB model of DFIG with control system.

Fig. 8 Generator speed for the applied wind speed

The controling of the stator active power to its refenece point is shown in Fig. 9.
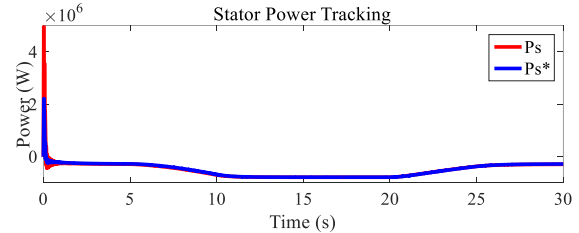

Fig. 9. Controlling the stator active power for maximum power tracking.

The minus sign is an indication of the generating mode of operation. In this modelling, the stator and grid side reactive power is set to zero for unity power factor of operation. The results of the simulation are shown in fig. 10 (a) and (b).
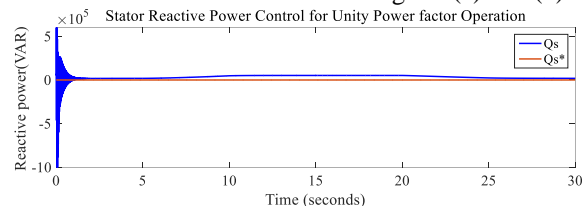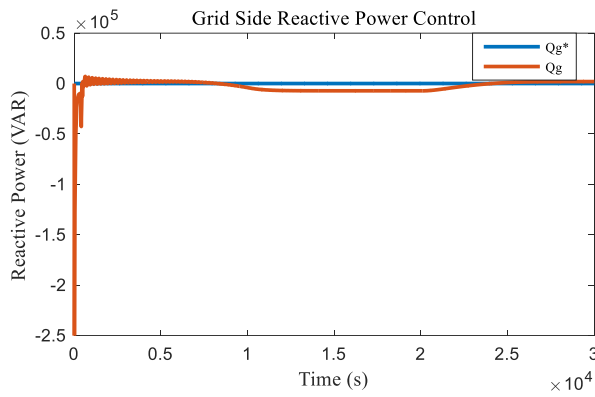

Fig.10 (a) Stator reactive power control at $Q_s*=0$.

Fig. 10 (b) GSC reactive power control at Q_g*=0.

As it is seen from Fig. 10 (a), the reactive power is not exactly tuned to zero at higher wind speed (10-20 seconds) of simulation period. Similarly, when the stator of the generator is delivering reactive power to the grid, the GSC is receiving it as shown in Fig. 10(b).

In both cases, the power factor is controlled to unity except at higher wind speeds. In addition, due to high switching frequency of the converters, there appear transients with grid side reactive power control during wind speed fluctuations.
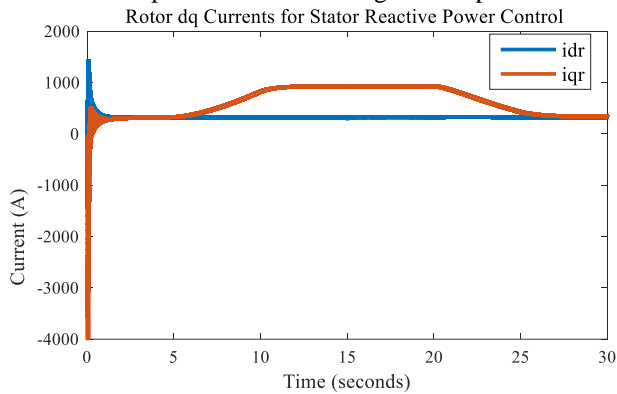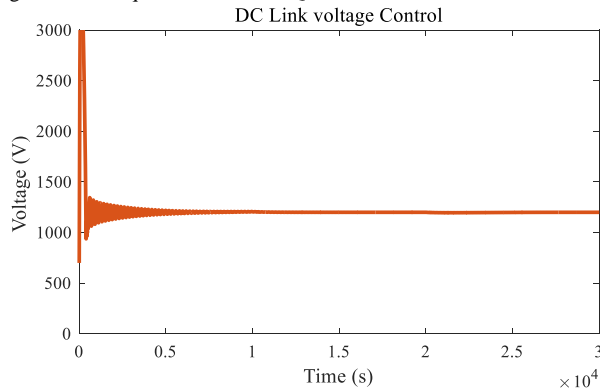

Fig. 11 Rotor dq-axis currents for Qs*=0

Fig. 12. DC Link voltage output

The d and q axis rotor currents are controlling the DFIG independently for stator reactive and active power respectively as shown in Fig. 11. The d axis current is set constant near 326 A for uniy power factor and the rotor q axis current traces its active power to get controlled.

The dc link voltage is made to be controlled at 1200 V and the result is shown in Fig. 12.

The PI controller of the dc link well adjusts the voltage to its reference value except with small perturbations at start up and when the wind speed gets changing.

For the purpose of comparision, the mechanical power of wind turbine, stator, rotor, and grid side converter (filter) powers are drawn together as shown in Fig. 13. As it is seen in Fig. 13, the wind turbine is generating near 1.1 MW at higher wind.
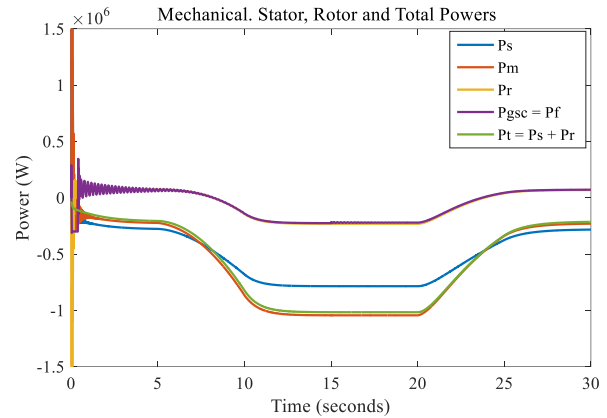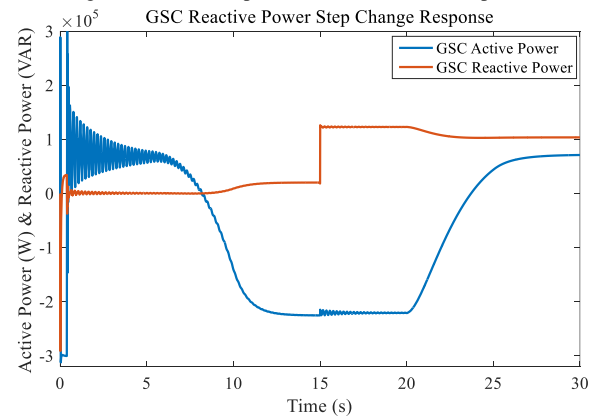

Fig. 13. Mechanical power with stator and rotor powers.

When Q_g is made to vary from 0 KVAR to 100KVAR at a time t = 15s as shown in Fig. 14 (a) with the dc bus reference voltage value held fixed and Q_s* is still held at zero, the system's response is shown in Fig. 14(b).

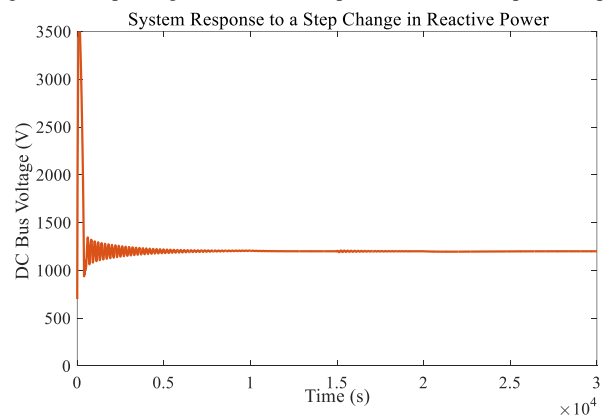Fig. 14 (a) Step change of GSC reactive power and its active power responses.

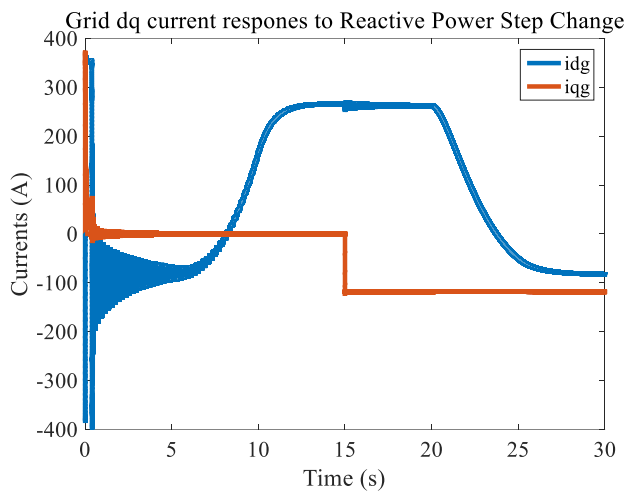Fig. 14 (b) System response for step change of GSC reactive power.

Fig. 14 (c) dq-axis currents for step change of reactive power.

There is a very small ripple in dc voltage during the change of reactive power, which is again reflected in the d-axis current reference as shown in Fig.14 (c) whereas, its change is reflected only in the change of q-axis of current. The d-axis current remains constant except with small perturbations. In addition, the grid side active power is maintained at the reference value constantly, and hence the maximum load current around 280 A is flowing at higher wind speed. This is an indication of an independentl control of d and q axis components for P_s and Q_s. Moreover, it is seen that the system works well even in case of change of reactive power flow.

On the other hand, when the load current at receiving end (grid) is changed from 0 to 286 A at a time t=15s as shown in Fig. 15(a) by keeping the dc voltage and grid side active power set as they are, the reactive power reference is set to zero, the effects is analysed. The grid side active and reactive power for the load change are shown in Fig. 15 (c)
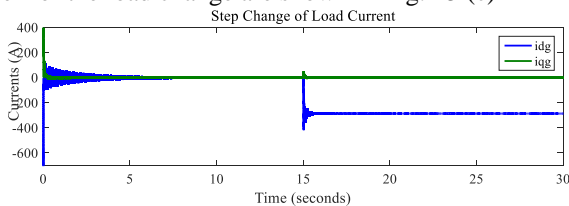

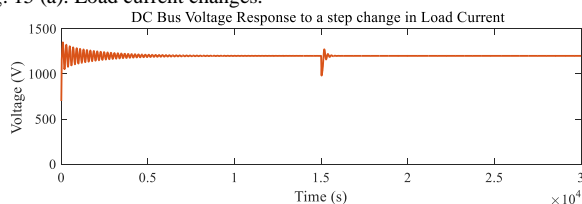Fig. 15 (a). Load current changes.

Fig. 15 (b). DC Link voltage response for load current changes.
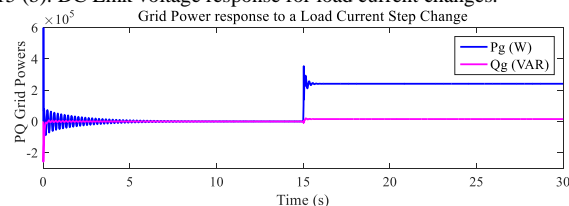

Fig. 15 (c). Active and reactive power responses to a load current changes.

From the responses as shown in Fig. 15 (b & c), it can be said that the system works stably with the changes of active power

as well. The step change also caused transients in dc voltage as shown in Fig. 15(c), but the step change in active power (load current) causes a much higher transient than that with the change in reactive power. Hence the decoupled control of active and reactive power is also ensured. The PI controller performs well in tracking the reference input. Thus, the DC bus is to be controlled at its reference point all the time so as to trace the changes in load currents and hence maintain controlled power flows.

VII. CONCLUSIONS

In this paper, the stator active and reactive powers of the machine are independently controlled by the designed PI controller with the aid of q and d axis currents of the rotor respectively. The stator power control is a very important issue now days with regard to grid code requirements of one's power system network as to allow unity power factor, active and reactive power demand control. The DC bus voltage control which is another important point for power flow control through the GSC is done with its own PI control gains. It was seen that the dc link voltage controller performs well with small perturbations even under load current variations which mainly occurs during voltage sag or dip as a result of faults in the power network where the study is further under way on it with. The dc bus system is analyzed for active and reactive power changes as well. In this study, the losses in converters and grid side filter, saturation of the machine, the stator resistance under the stator flux orientation and other related losses are neglected and needs to be remarked for some small variations.

VIII. REFERENCES

[1] Dr. Jasper Abramowski, Dr. Rolf Posorski, "*Wind Energy for Developing Countries*," DEWI Magazine Nr. 16, GTZ, Germany, 2000,

[2] http://allafrica.com/stories/201505211503.html [online]

[3] G. Abad, J. Lo´pez, M. A. Rodri´guez, L.Marroyo, and G. Iwanski, "*Doubly Fed Induction Machine: Modeling and Control for Wind Energy Generation*," First Edi., IEEE Press and John Wiley and Sons Ltd., 2011

[4] Kundur, P. (1994), "*Power System Stability & Control*," EPRI, McGraw-Hill, New York.

[5] H. Abu-Rub, M. Malinowski & K. Al-Haddad (), "*Power Electronics for Renewable Energy Systems, Transp.& Indus. Applns.,*" 1st Edi., IEEE Press and John Wiley and Sons Ltd., 2014

[6] SANY 1.5 MW series WTG product manual of Adama-II wind farm ''unpublished'.

[7] Sany DFIG Ethiopia Adama-II wind power project test report ''unpublished''.

[8] O.Lara, Nick Jenkins, Janaka Ekanayake, Phill Cartwright, Mike Hughes, "*Wind Energy Generation Modeling and Control,*" John Wiley and Sons Ltd., Publication, 2009

[9] Milkias Berhanu, Robert Leidhold, Zenachew Muluneh, Yemeserach Mekonnen, and Arif Sarwat, 'Real-Time Control of a Doubly-Fed Induction Machine for Variable Speed Constant Frequency Wind Power System Through Laboratory Test Rig,' 2018 IEEE PES/IAS PowerAfrica, 978-1-5386-4163-7/18/$31.00 ©2018 IEEE

[10] M. Berhanu, Y. Mekonnen, R. Leidhold, M. Mamo, Z. Muluneh, and A. Sarwat, 'Analysis of a Doubly Fed Induction Generator Through Modeling and Simulation,' 2018 IEEE PES-IAS PowerAfrica, 978-1-5386-4163-7/18/$31.00 ©2018 IEEE.